



**HAL**  
open science

## New models for ultrasonic guided wave inspections in CIVA

V. Baronian, K. Jezzine, N. Dominguez, Sylvain Chatillon

► **To cite this version:**

V. Baronian, K. Jezzine, N. Dominguez, Sylvain Chatillon. New models for ultrasonic guided wave inspections in CIVA. NDT 2013 - 52nd Annual Conference of the British Institute of Non-Destructive Testing 2013, Sep 2013, Telford, United Kingdom. pp.488-499. cea-01844701

**HAL Id: cea-01844701**

**<https://cea.hal.science/cea-01844701>**

Submitted on 22 Jan 2024

**HAL** is a multi-disciplinary open access archive for the deposit and dissemination of scientific research documents, whether they are published or not. The documents may come from teaching and research institutions in France or abroad, or from public or private research centers.

L'archive ouverte pluridisciplinaire **HAL**, est destinée au dépôt et à la diffusion de documents scientifiques de niveau recherche, publiés ou non, émanant des établissements d'enseignement et de recherche français ou étrangers, des laboratoires publics ou privés.

## **New models for ultrasonic guided wave inspections in CIVA**

Vahan Baronian, Karim Jezzine, Nicolas Dominguez, Sylvain Chatillon  
CEA, LIST  
F-91191, Gif-sur-Yvette France  
Tel +33169086384  
Fax +33169087597  
Vahan.baronian@cea.fr

### **Abstract**

Models for ultrasonic guided wave NDT are developed at CEA LIST and integrated into the CIVA platform. Models already available in CIVA 10 deal with plates and cylindrical guides, possibly multilayered. Mode computation, radiated field from different type of transducers (contact with or without wedge, surrounding or surrounded arrays in pipes) and response of a NDT examination in pulse-echo or pitch-catch configurations for a crack orthogonal to the guide axis are proposed. These models are now extended to deal with guides of arbitrary section with planar extrusion, modes being computed with the Semi-Analytical Finite Element (SAFE) method. A hybrid SAFE-Finite Element method has also been integrated to compute the response of a flaw of arbitrary shape, a weld or a complex junction. These new models as well as their validations are presented and discussed.

### **1. Introduction**

Simulation tools for guided wave inspection are being developed at CEA LIST. These tools aim at designing and optimising NDT methods or probes, or interpreting experimental data. The developed models are based on a modal decomposition. In practice, the knowledge of mode behaviour and dispersion characteristics is an essential step for understanding complex phenomena arising in a guide. Measured or simulated signals are then interpreted in reference to modes. Typical questions concern the ability of modes to be transmitted through or reflected on a guide discontinuity, to be converted into other modes in the interaction. Simulations are thus performed in the frequency domain and are subsequently synthesized by Fourier transform over a limited spectrum.

At a given frequency, the elastodynamic field (particle displacement or velocity, stress) can be decomposed as a linear combination of eigenmodes computed in the cross-section of the structure whose guiding axis is taken as  $x_3$ . The  $n^{\text{th}}$  mode of this set is described at a given frequency by: i) its wavenumber  $\beta_n$ , real for the finite number of

propagative modes, imaginary for the finite number of evanescent modes or includes an imaginary part for the infinite number of inhomogeneous modes, ii) the corresponding particle displacement vector  $\mathbf{u}^n(\mathbf{x}_S)$  in the invariant cross-section of the waveguide,  $\mathbf{x}_S$  denotes the position in the cross section. The displacement  $\mathbf{u}(\mathbf{x}; t)$  at any position  $\mathbf{x} = (x_1, x_2)$  in the waveguide at the pulsation  $\omega$  is expressed by:

$$\mathbf{u}(\mathbf{x}; t) = \sum_n A_n \mathbf{u}^n(\mathbf{x}_S) e^{j(\beta_n x_3 - \omega t)}$$

where  $A_n$  denotes the  $n^{\text{th}}$  amplitude coefficient in the decomposition.

A given mode may be transmitted through or reflected on a guide discontinuity or partially converted into other modes in the interaction. The modal description is used in the regular parts of the waveguide, whereas models for transduction or scattering by guide discontinuities or flaws are used locally. To compute modal solutions, the semi-analytical finite element method has been implemented <sup>(1)</sup>. This method allows the computation of both wavenumbers  $\beta_n$ , and modal displacements  $\mathbf{u}^n(\mathbf{x}_S)$ . It can deal with waveguides of arbitrary section and anisotropic materials.

The computation of modal amplitudes emitted by a transducer may be performed under the assumption that piezo-transducers can be modelled as sources of normal or tangential stresses over their active surface. For a transducer acting from the guiding surface, a Green function for a given mode is derived and a surface integration over the transducer performed <sup>(2)</sup>.

The scattering problem is written in the form of a matrix of complex coefficients  $R_{nm}$  and  $T_{nm}$ , assuming that modal solutions in guiding structures connected to the local zone of scattering are known.  $R_{nm}$  (resp.  $T_{nm}$ ) is the reflection (resp. transmission) coefficient for the incident  $m^{\text{th}}$  mode and the reflected (resp. transmitted)  $n^{\text{th}}$  mode. They stand for the scattering by an inhomogeneity of the guide. This matrix links an input vector constituted by the modal coefficients of the incoming wave, to output vectors constituted by those of the outgoing waves. For planar crack-like defects of arbitrary shape in an otherwise homogeneous guide, assuming that crack surface belongs to the guide cross-section, a mode matching method can be performed to compute the scattering matrix <sup>(3)</sup>.

## 2. Simulations based on hybrid SAFE-FE method

### 2.1 Theory

To deal with arbitrary flaw shapes, guide inhomogeneities or junctions between several guides, a finite element (FE) scheme has been developed with the further goal to limit the computation zone to a minimal size for efficiency <sup>(4)</sup>. The computation relies on the use of artificial boundary conditions endowing transparency. Radiation conditions at infinity are brought back to the artificial boundaries by building an operator coupling the finite elements inside the FE zone to modal solutions in guides. An original mixed formulation has been derived whose unknowns are the displacement field in the bounded domain and the normal component of the normal stresses on the artificial

boundaries. The scattered field is then projected on modal solutions in guides through the use of bi-orthogonality relations. This method has been established for 2D and 3D waveguides in Cartesian coordinates. It can deal with the scattering by a junction made up of an arbitrary number of waveguide<sup>(5)</sup>. In the next release of CIVA GW software, only the 2D (dealing with the scattering of Lamb wave) and axisymmetric version are implemented.

The main steps of the hybrid method are recalled, in particular the building of transparent boundary conditions by using the bi-orthogonality relation of Fraser expressed in terms of the so-called mixed vectors  $\mathbf{X}$  and  $\mathbf{Y}$ , first introduced by Pagneux and Maurel<sup>(6)</sup>. This relation is the key point of the method since it allows projecting the scattering field on the modal decomposition. A complex junction  $\Omega$  between  $N$  waveguides is represented on Figure 1. A bounded domain  $\Omega$  connected to an arbitrary number  $N$  of different waveguides on its boundaries  $\Sigma_k, (1 \leq k \leq N)$  is considered.

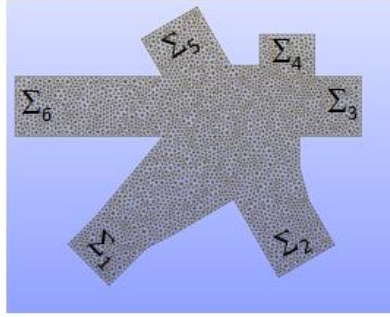


**Figure 1.** A complex scattering junction  $\Omega$  connected to  $N$  uniform waveguides.

The aim of the coupling method is to build modal transparent boundary conditions on the interfaces  $\Sigma_k$  of the computational domain  $\Omega$  for the diffracted waves.

Let's consider an incident right-going mode  $n_0$  on the interface  $\Sigma_1$  at  $\mathbf{x}^l = (x_3^l, x_3^l)$ :

$$\mathbf{u}^{inc}(\mathbf{x}^l) = \mathbf{u}^{l,n_0}(\mathbf{x}_5^l) e^{j\beta_{n_0}^l (x_3^l - x_3^l|_{\Sigma_1})},$$

The diffracted displacement field  $\mathbf{u}^{dif}(\mathbf{x}) = \mathbf{u}^{tot}(\mathbf{x}) - \mathbf{u}^{inc}(\mathbf{x})$  can be expressed by a sum over the outgoing waves using the modal decomposition in each uniform waveguide  $\Sigma_k$ :

$$\mathbf{u}^{dif}(\mathbf{x}) = \sum_k \sum_n A_{k,s_k n}^{dif} \mathbf{u}^{k,s_k n}(\mathbf{x}_5^k) e^{s_k j\beta_n^k (x_3^k - x_3^k|_{\Sigma_k})},$$

where  $s_k$  denotes the sign (+ or -) of propagation for the diffracted waves,  $A_{k,s_k n}^{dif}$  the magnitude of the  $n^{th}$  outgoing mode,  $\mathbf{x}_5^k$  the local transverse coordinates,  $x_3^k$  the local axial coordinate and  $x_3^k|_{\Sigma_k}$  the local axial position of the boundary  $\Sigma_k$ , for each uniform waveguide  $N_k$ .

$\mathbf{X}$  is composed by the transverse component of the normal stress and the axial component of the displacement field, whereas  $\mathbf{Y}$  (the dual of  $\mathbf{X}$ ) is composed of the transverse component of the displacement field and the opposite of the axial component of the normal stress:

$$\mathbf{X} = \begin{pmatrix} t_S \\ u_3 \end{pmatrix}, \mathbf{Y} = \begin{pmatrix} u_S \\ t_3 \end{pmatrix}$$

Fraser's relation expressed in term of  $\mathbf{X}$  and  $\mathbf{Y}$  corresponds to an orthogonality relation between two modes  $n$  and  $m$  that propagate in the same direction:

$$(\mathbf{X}^n | \mathbf{Y}^m)_S = (t_S^n u_S^m + t_3^m u_3^n)_S = J_n \delta_{nm},$$

where  $(\cdot)_S$  denotes the integration over the cross-section of the waveguide and  $\delta_{nm}$  is the Kronecker symbol.

The mixed variables  $\mathbf{X}$  and  $\mathbf{Y}$  for the diffracted field can be similarly expanded thanks to the modal decomposition:

$$\begin{pmatrix} \mathbf{X}^{dif}(\mathbf{x}) \\ \mathbf{Y}^{dif}(\mathbf{x}) \end{pmatrix} = \sum_k \sum_n A_{k,s_k n}^{dif} \begin{pmatrix} \mathbf{X}^{k,s_k n}(\mathbf{x}_S^k) \\ \mathbf{Y}^{k,s_k n}(\mathbf{x}_S^k) \end{pmatrix} e^{s_k j \beta_n^k (x_S^k - x_{\Sigma}^k)}$$

Using the bi-orthogonality relation, the amplitude  $A_{k,s_k n}^{dif}$  of the  $n^{th}$  mode can be recovered as follow:

$$A_{k,s_k n}^{dif} = (\mathbf{X}_{\Sigma_k}^{dif} | \mathbf{Y}^{k,s_k n})_S = (\mathbf{Y}_{\Sigma_k}^{dif} | \mathbf{X}^{k,s_k n})_S$$

Introducing the expression of  $A_{k,s_k n}^{dif}$  in the previous modal expansion, one expresses two coupling operators  $\mathbf{XtY}$  and  $\mathbf{YtX}$  (similar to DtN, for Dirichlet-to-Neumann) mapping the trace of  $\mathbf{X}_{\Sigma_k}^{dif}$  to the trace of  $\mathbf{Y}_{\Sigma_k}^{dif}$  on each boundary  $\Sigma_k$  or vice-versa:

$$\begin{pmatrix} \mathbf{X}_{\Sigma_k}^{dif} \\ \mathbf{Y}_{\Sigma_k}^{dif} \end{pmatrix} = \sum_n \begin{pmatrix} (\mathbf{Y}_{\Sigma_k}^{dif} | \mathbf{X}^{k,s_k n})_S \mathbf{X}^{k,s_k n}(\mathbf{x}_S^k) \\ (\mathbf{X}_{\Sigma_k}^{dif} | \mathbf{Y}^{k,s_k n})_S \mathbf{Y}^{k,s_k n}(\mathbf{x}_S^k) \end{pmatrix}$$

Now using one of these so-called boundary maps, it is possible to formulate the diffraction problem in the bounded domain  $\Omega$  where the transparent boundary conditions on the section  $\Sigma_k$  will be expressed by the means of the chosen coupling operator  $\mathbf{XtY}$  or  $\mathbf{YtX}$ . They correspond to an outgoing wave condition for the computational domain  $\Omega$ . This condition represents a modal transparent boundary condition for guided waves.

The diffraction problem is then formulated by a variational formulation where the unknown is the total displacement field  $\mathbf{u}^{tot}$ . To express the boundary terms on the section  $\Sigma_k$  corresponding to the work of the external stresses on the boundaries  $\Sigma_k$ , the part of the coupling operator related to the stresses components ( $t_{S|\Sigma_k}$  for  $\mathbf{YtX}$  or  $t_{3|\Sigma_k}$  for  $\mathbf{XtY}$ ) is introduced. The corresponding missing stress component ( $t_{3|\Sigma_k}$  for  $\mathbf{YtX}$  or  $t_{S|\Sigma_k}$  for  $\mathbf{XtY}$ ) as a Lagrange's multiplier is subsequently introduced. This leads to a mixed variational formulation where unknowns correspond to the total displacement field and the  $N_k$  Lagrange's multipliers. Moreover, as we have introduced  $k$  Lagrange's multipliers, we need  $k$  more equations to complete the variational system, which is done

by expressing a weak variational formulation of the remaining equations issued from the coupling operator ( $u_{3|\Sigma_k}$  for  $YtX$  or  $u_{s|\Sigma_k}$  for  $XtY$ ). More precisely this corresponds to the compatibility between the corresponding displacement component (axial  $u_{3|\Sigma_k}$  or transverse  $u_{s|\Sigma_k}$ ) given by the finite element representation and its modal representation (on the artificial boundaries).

Scattering coefficients can finally be expressed in term of reflection and transmission coefficient:

$$T_{nm}^{kl} = \left( X_{\Sigma_k}^{tot} | Y^{k,n} \right)_{\Sigma_k} / \left( X_{\Sigma_l}^{inc} | Y^{l,m} \right)_{\Sigma_l}$$

$$R_{nm}^{ll} = \left( X_{\Sigma_l}^{tot} - X_{\Sigma_l}^{inc} | Y^{l,-n} \right)_{\Sigma_l} / \left( X_{\Sigma_l}^{inc} | Y^{l,m} \right)_{\Sigma_l}$$

## 2.2 Simulation of the interaction of Lamb wave with a complex junction

A first example is proposed to illustrate the capabilities of the hybrid SAFE-FE method. The junction of six steel plates is shown on figure 2. A wedge transducer is positioned on a 50mm thick branch and radiates Lamb wave through the junction. A similar transducer acts as a receiver on the other side of the junction 700 mm from the emitter. The emitter is driven by a narrow band excitation composed of 20 cycles modulated by a Hanning window at 110 kHz. The angle of both wedge transducers is set arbitrarily at 31°. The mesh used for the FE computation, as well as the distribution of energy among the different existing modes in the excitation branch are also shown on Figure 2.

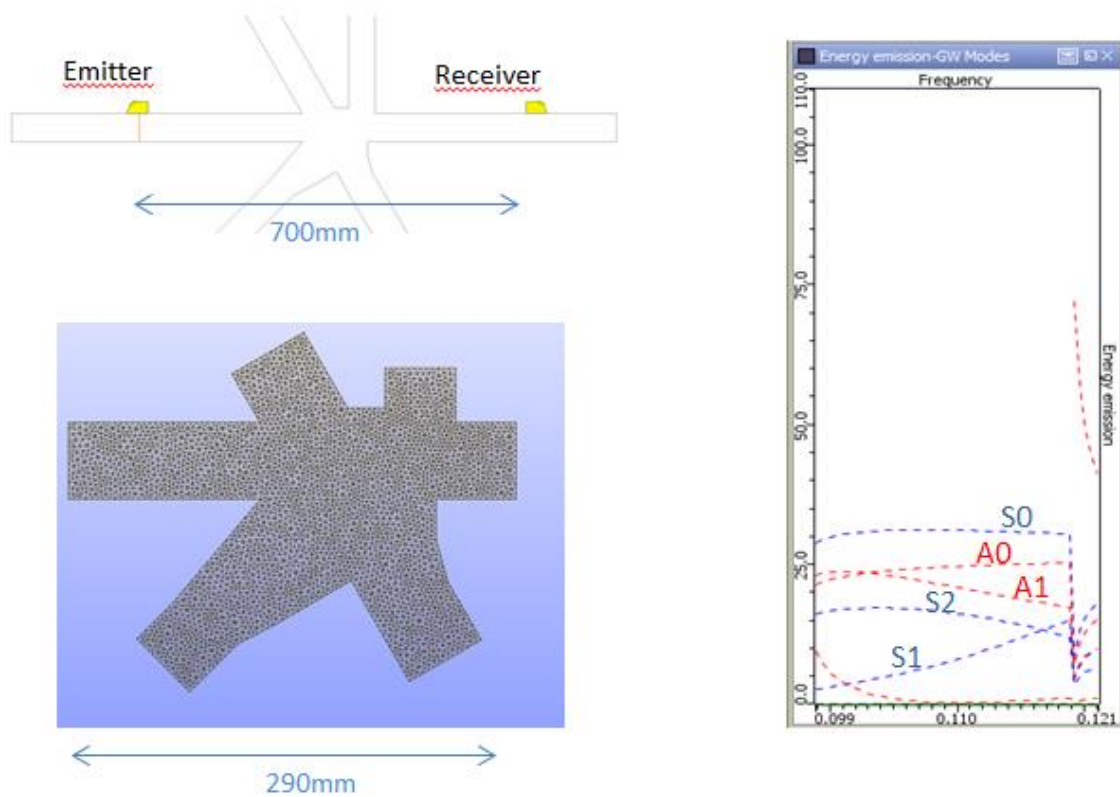


**Figure 2.** Inspection of a complex junction connecting six uniform waveguides (top left). FE meshing of the junction (bottom left). Distribution (percentage) of incident

*energy in the left branch among symmetric and antisymmetric modes around the transducer centre frequency (right).*

Snapshots of the displacement wavefield inside the FE box are represented on Figure 3. A comparison between received signals obtained in presence of the complex junction and in the case of a simple plate of 50mm thickness shows that the junction induces a loss of 13 dB (Figure 4).

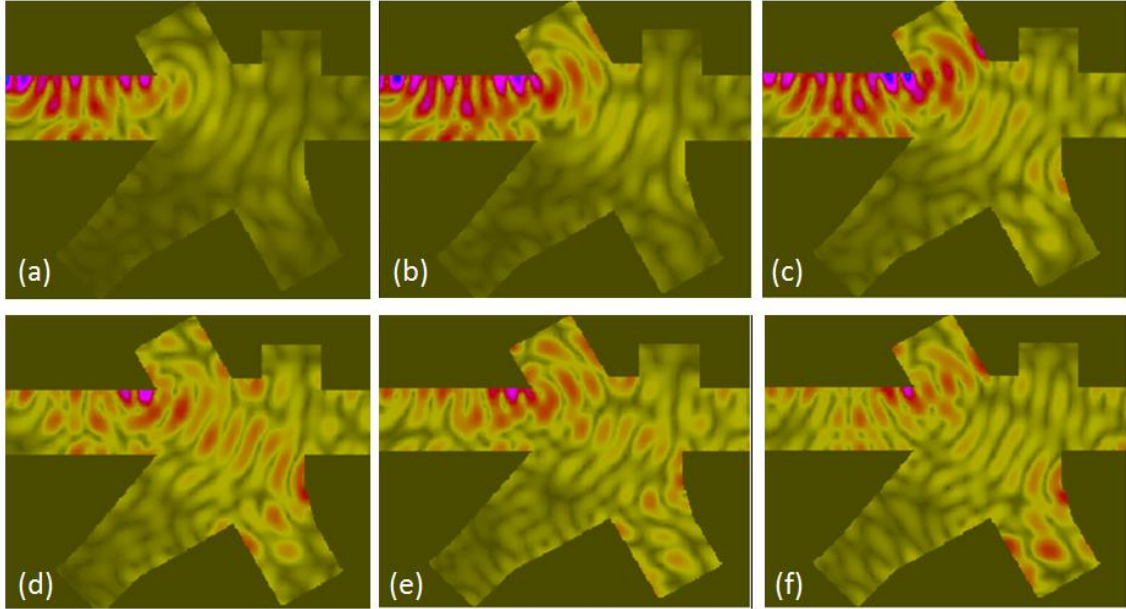


**Figure 3.** Snapshots of displacement wavefield inside the junction at  $t=350\mu\text{s}$  (a),  $t=385\mu\text{s}$  (b),  $t=420\mu\text{s}$  (c),  $t=455\mu\text{s}$  (d),  $t=490\mu\text{s}$  (e) and  $t=525\mu\text{s}$  (f).

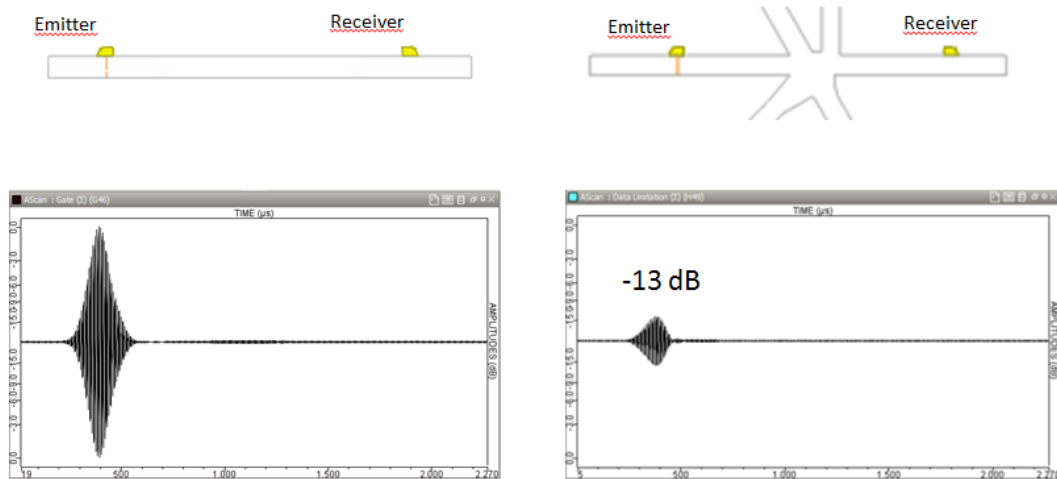


**Figure 4.** Simulated waveform measured on the receiver in a uniform plate (left) and after crossing the junction (right)

### 2.3 Simulation of the interaction of Lamb wave with corrosion-pitting

In this section, the interaction of Lamb modes with corrosion pitting in a 2mm thick aluminium plate is simulated. Material properties used are  $\rho=2700\text{kg/m}^3$ , Lamé's coefficient  $\mu=0.2662\times 10^{11}$  Pa and  $\lambda=0.5597\times 10^{11}$  Pa. A similar study has been performed by Terrien *et al.* <sup>(7)</sup> to detect the presence of corrosion in aircraft structures. The basic idea is to use Lamb modes at relatively high frequency to detect early corroded areas. Indeed, at high frequencies, Lamb modes are more sensitive to corrosion microstructure than to thickness variations, which may allow corrosion to be discriminated from plate thinning. Corrosion pits are modelled by a distribution of cracks of 100  $\mu\text{m}$  depth and width (Figure 5). Two identical wedge transducers are positioned on each side of the corroded area, 200 mm from each other. The emitter is driven by a narrow band excitation composed of 20 cycles modulated by a Hanning window at 2 MHz. As the angle of the wedge transducers are adjusted to match the phase velocity of the S0 mode at 2MHz, only the fundamental symmetric mode S0 is incident on the corrosion area and the receiving probe detects essentially the same mode. This is confirmed by the simulation of the distribution of energy carried by the five existing modes in the transducer frequency bandwidth (S0, S1, S2, A0 and A2) shown on Figure 6.

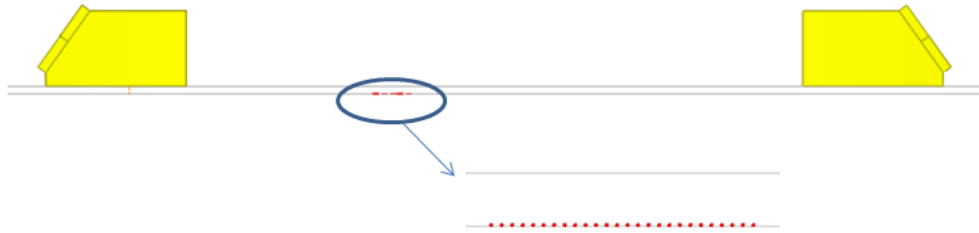


**Figure 5. Inspection of a 2-mm thick corroded aluminium plate. In this pitch-catch configuration, corrosion pits are modelled with a distribution of 100µm square notches. The distance between emitter and receiver is 200mm.**

Simulations of inspections have been performed with a length of corroded area ranging from 2mm to 10mm, its depth being set to 100µm. The amplitude of the received signal, as shown on Figure 7, decreases with the length of the corroded area. These results are in accordance with Terrien *et al.* <sup>(7)</sup>. Indeed, the presence of a corroded area induces a conversion from S0 mode to A0 mode, as shown on Figure 7. This conversion is found to be proportional to the length of the corroded area. The receiver being only sensitive to S0 mode, this explains the decrease of the received signal with the length of the corroded area.

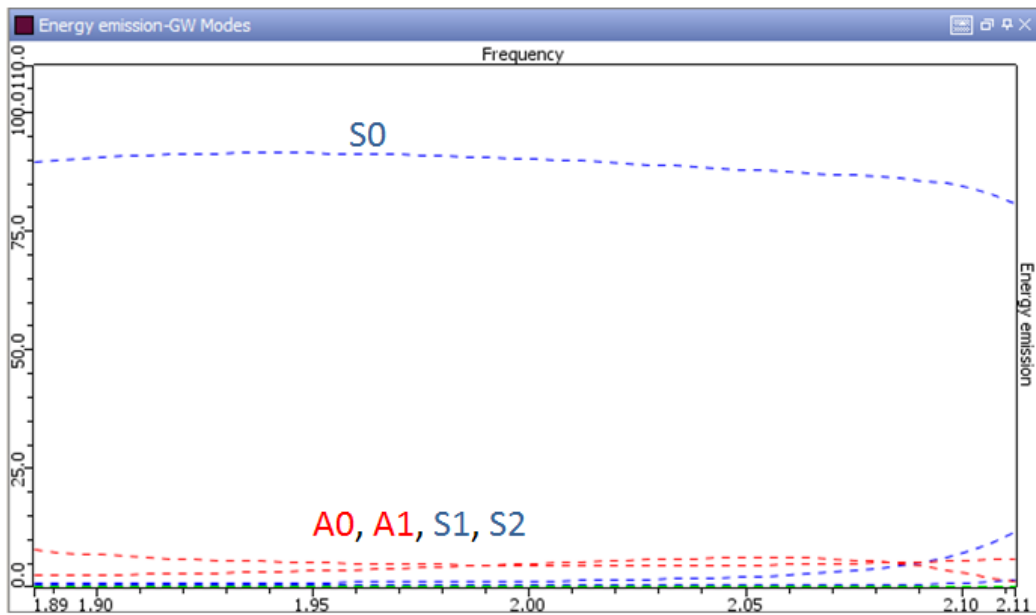


**Figure 6. Distribution (percentage) of energy among existing modes in the emitting wedge transducer frequency bandwidth. At 2MHz, around 90% of the energy is carried by the S0 mode.**

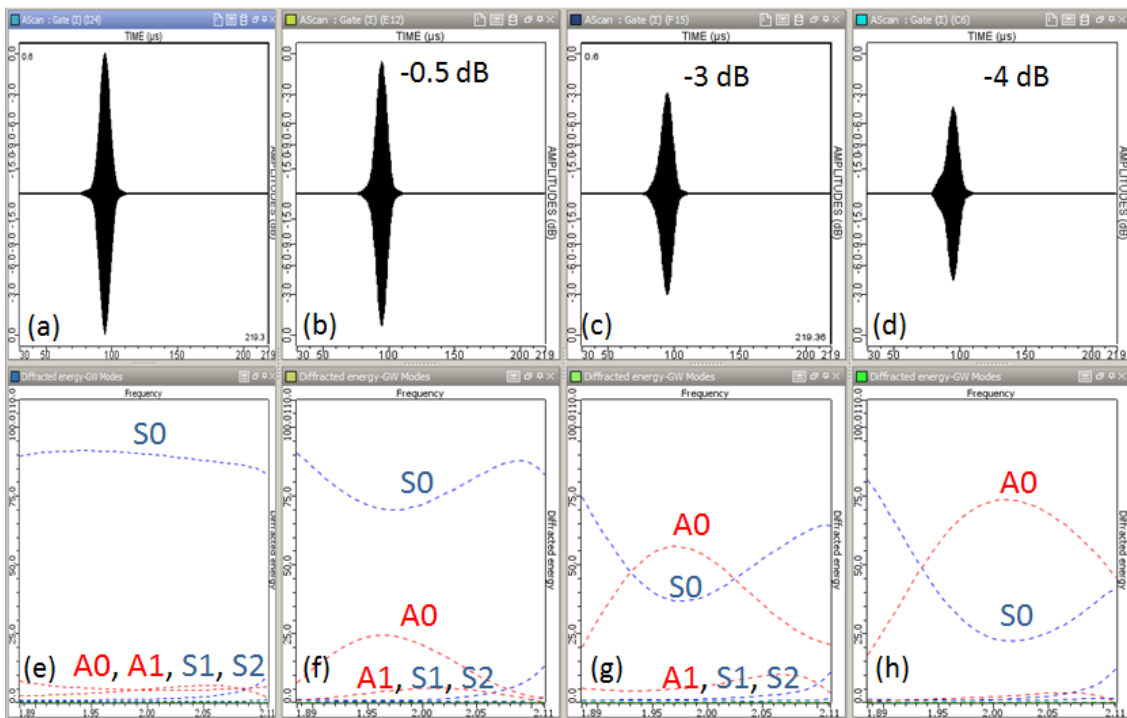


**Figure 7. Simulated waveform on the receiver for a healthy 2mm thick plate (a) and a plate with a corroded area of 2mm length (b), 5mm length (c), 10mm length (d). Distribution of transmitted energy towards the receiver (percentage) among existing modes for a healthy plate (e) and a plate with a corroded area of 2mm length (f), 5mm length (g), 10mm length (h).**

The interaction of Lamb wave with a thickness variation has also been investigated. For a 10 mm long and 100 $\mu$ m deep plate thinning corresponding to the same thickness as corrosion pittings considered previously, the received signal (Figure 8a) is very close to the one obtained for a healthy plate (Figure 7a). Indeed, nearly no mode conversion occurs in this case (Figure 8c). This allows a 10 mm long corroded area (Figure 8b and 8d) to be discriminated from a plate thinning of similar extent.

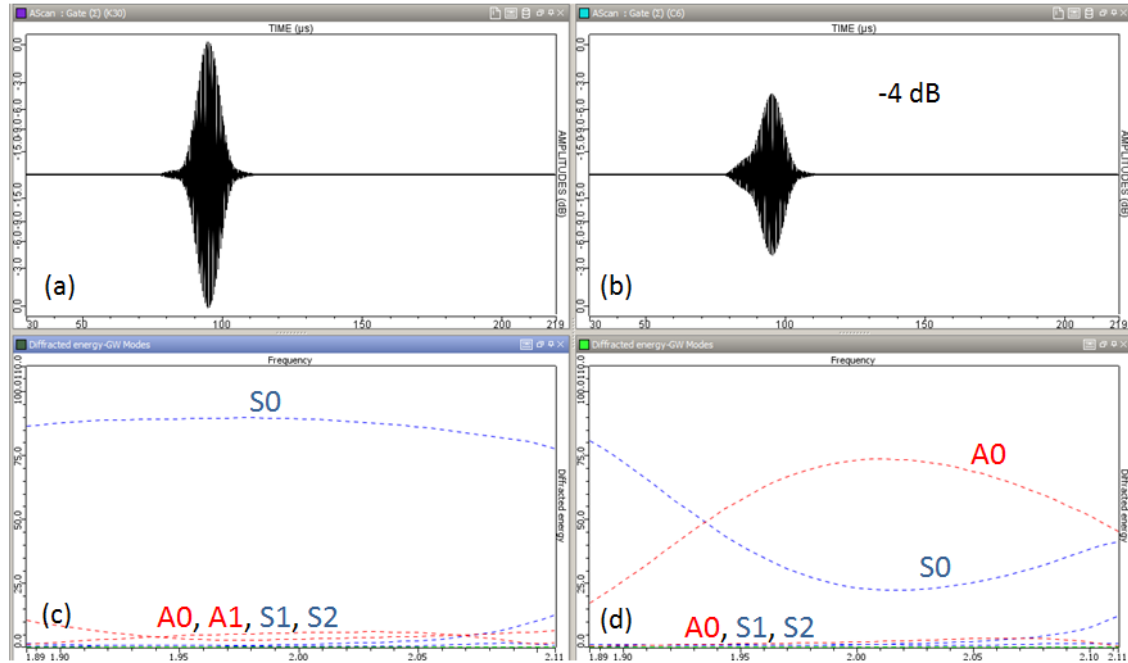


**Figure 8. Simulated waveform on the receiver and distribution of transmitted energy towards the receiver after diffraction by a 100 $\mu$ m deep and 10 mm long plate thinning (a and c) or 100 $\mu$ m deep and 10mm long corroded area (b and d)**

### 3. Mode and field computation in guides of arbitrary section

#### 3.1 Theory

The semi-analytical finite element method (SAFE) <sup>(1)</sup> allows the computation of both wave vectors and modal displacements in the section as being the eigenvalues and eigenvectors (resp.) of a quadratic system of equations. This system is the discrete form of a variational problem in the guide section. Since it is based on a finite element discretisation of the section, it allows one to deal with all sorts of guide characteristics (shape, constitutive materials). Specifically, multilayered structures, anisotropy and viscoelasticity can be easily accounted for. We have implemented this method to deal with various guiding structures. Guide section is meshed either by 1D linear element for plates, cylinders or tubes, or 6-noded triangular finite elements in the general case of arbitrary section. As the mesh is restricted to the section, the method is computationally very efficient

### 3.2 Simulation of mode and field computation in a rail

The wavefield emitted by a piezo transducer in a steel rail structure has been computed with the SAFE method (see configuration on Figure 9). The emitter is driven by a narrow band excitation composed of 10 cycles modulated by a Hanning window at 40 kHz.

Phase and group velocities dispersion curves up to 100 kHz are shown on Figure 10 as well as displacement and stress for arbitrary mode and frequency.

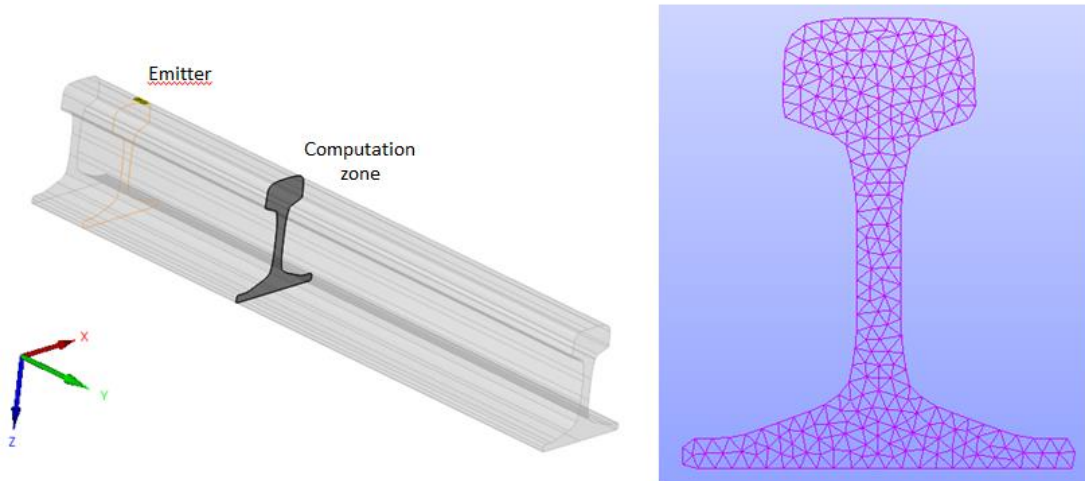


Figure 9. Inspection configuration of a rail and FE mesh used for the SAFE computation. Rail dimensions are 150 mm width and 172 mm height. The computation is positioned 1m from the piezo emitter

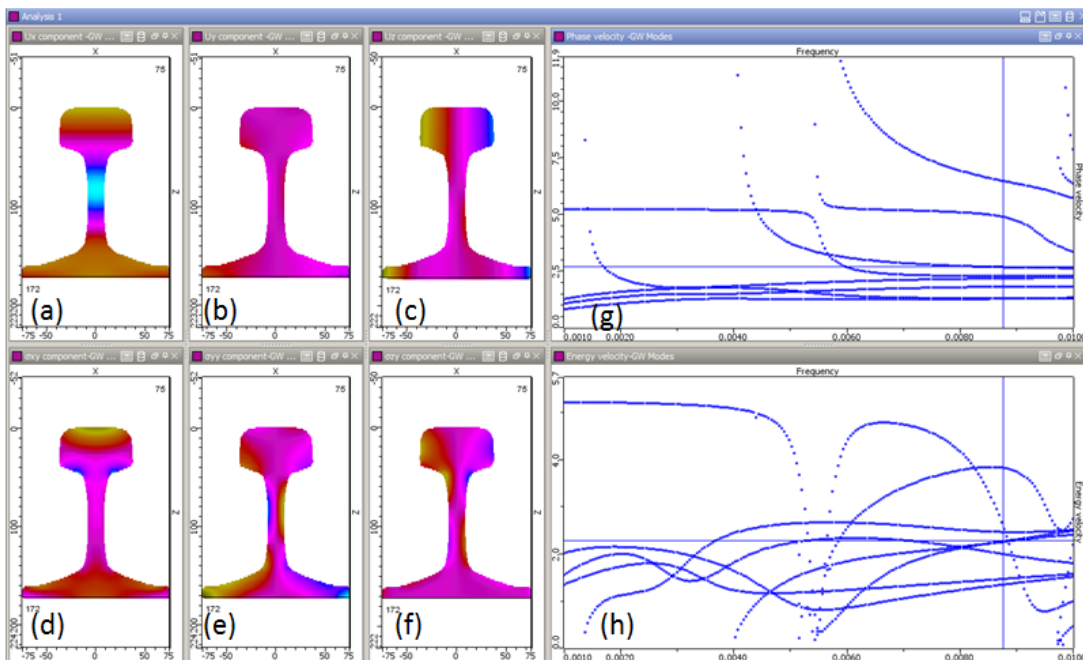
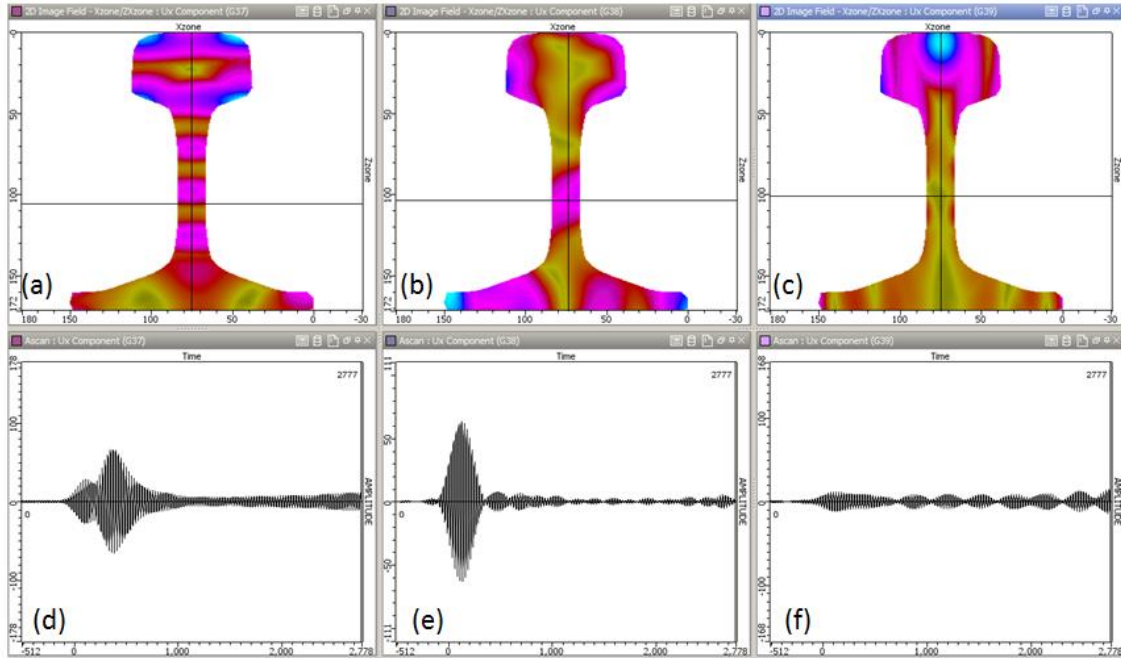


Figure 10. Computation of guided modes in a rail. Phase velocity (g) and group velocity (h) dispersion curves. Displacement components (a,b,c) and stress components (d,e,f) in the section at an arbitrary location on the dispersion curves.

The maximum of displacement in the computation zone corresponding to a cross-section located 1m away from the emitter is shown on Figure 11 as well as time waveforms simulated near the centre of the rail.



**Figure 11. Maximum of displacement along X (a), Y (b) and Z (c) in the computation zone defined on Figure 9. Simulated waveforms near the centre of the rail, corresponding to the displacement along X (d), Y(e) and Z (f).**

## 5. Conclusions

Models for GW / NDT simulation have been described. A specific FE method has been derived for computing the scattering by arbitrary flaw shapes, guide inhomogeneities or junctions between several guides. It includes exact transparent artificial boundaries for minimizing the size of the FE zone, thus reducing computation costs. A 2D version for plates and an axisymmetric version for pipes has been implemented in CIVA. The SAFE method has also been implemented to deal with guided propagation in uniform guides of arbitrary section. In addition, the simulation of pipe inspection can now handle the presence of inner fluid and an algorithm for the computation of amplitude and delay laws for phased array in pipes is now proposed in CIVA.

## References

1. S.B. Dong and R.B. Nelson, 'On Natural Vibrations and Waves in Laminated Orthotropic Plates', *J. Appl. Mech.*, Vol. 39, pp. 739-745, 1972.
2. J. Li and J.L. Rose, 'Excitation and Propagation of Non-Axisymmetric Guided Waves in a Hollow Cylinder', *J. Acoust. Soc. Am.*, Vol. 109, pp. 457-464, 2001.
3. K. Jezzine and A. Lhémery, 'Simulation of Guided Wave Inspection Based on the Reciprocity Principle and the Semi-Analytical Finite Element Method', *Review of Progress in QNDE*, Vol. 26, pp. 39-46, 2007.
4. V. Baronian, A.-S. Bonnet-BenDhia, A. Lhémery and É. Lunéville, 'A Numerical Method for the Simulation of NDT Experiments in an Elastic Waveguide', *Springer Proceedings in Physics*, Vol 128, pp 137-147, 2009.
5. V. Baronian, A. Lhémery and K. Jezzine, "Hybrid SAFE/FE Simulation of Inspections of Elastic Waveguides Containing Several Local Discontinuities or Defects", *Review of Progress in QNDE*, Vol 30, pp 183-190, 2011.
6. V. Pagneux and A. Maurel, "Lamb wave propagation in inhomogeneous elastic waveguides", *Proc. R. Soc. Lond. A*, Vol 458, pp. 1913–1930, 2002.
7. N. Terrien, D. Osmont, D. Royer, F. Lepoutre and A. Déom, 'A combined finite element and modal decomposition method to study the interaction of Lamb modes with micro- defects', *Ultrasonics*, Vol 46, pp 74-88, 2007.